Enhanced energy extraction via magnetic reconnection in Kerr-AdS spacetime*

Bo Zhao (赵博) Chao-Hui Wang (王朝辉) Shao-Wen Wei (魏少文)†

[1]Key Laboratory of Quantum Theory and Applications of MoE, Lanzhou University, Lanzhou 730000, China
[2]Lanzhou Center for Theoretical Physics, Key Laboratory of Theoretical Physics of Gansu Province, School of Physical Science and Technology, Lanzhou University, Lanzhou 730000, China
[3]Institute of Theoretical Physics & Research Center of Gravitation, Lanzhou University, Lanzhou 730000, China

Abstract: In this study, we examine the energy extraction from Kerr-AdS black holes following the magnetic reconnection process. The parameter space regions that satisfy the energy extraction condition, as well as the efficiency and power of the extracted energy, are analyzed. This study shows that the presence of a negative cosmological constant extends the range of dominant reconnection radial locations where the energy extraction condition is met and enables energy extraction, even from black holes with relatively low spin. Furthermore, the influence of the negative cosmological constant on energy extraction is modulated by the extent of the dominant reconnection radial region: a more negative cosmological constant enhances the extracted energy, efficiency, and power, particularly for smaller dominant reconnection radii. These results demonstrate that the energy extraction from Kerr-AdS black holes is more favorable than that from their asymptotically flat counterparts. Our results highlight the crucial role of the cosmological constant in energy extraction via magnetic reconnection.

Keywords: classical black hole, magnetic reconnection, energy extraction, cosmological constant

DOI: 10.1088/1674-1137/ae3db5 **CSTR:** 32044.14.ChinesePhysicsC.50055102

I. INTRODUCTION

Black holes, among the most enigmatic predictions of general relativity, are ultracompact objects whose extreme spacetime curvature prevents even light from escaping beyond the event horizon. Gravitational waves [1−3] and black hole images [4, 5] have recently been observed, confirming the existence of black holes. In astrophysical phenomena, astrophysical black holes are believed to be closely related to high-energy astrophysical phenomena, such as active galactic nuclei (AGN) [6−9] and ultraluminous X-ray binaries [10−12]. Therefore, the study of how black holes generate large amounts of relativistic jets and ultraluminous X-ray is a highly valued and ongoing research topic. Subsequent study has shown that the rotational energy of black holes can be regarded as one of the possible sources of the vast amount of energy released by these high-energy astrophysical phenomena.

The seminal work by Penrose first showed that rotational energy extraction from Kerr black holes could occur via the Penrose process, exploiting the existence of negative energy orbits in the ergosphere [13]. Subsequent developments by Piran and Shaham introduced the collisional Penrose process in 1975 [14], in which two particles collide within the ergosphere to produce two new particles, one of which is captured by the black hole while the other escapes the black hole and returns to infinity. This mechanism was later extended by Banados, Silk, and West, who demonstrated that extremal Kerr black holes could serve as Planck-scale particle accelerators through the Banados-Silk-West (BSW) effect to extract energy from black holes [15]. In addtion, Blandford and Znajek proposed a mechanism, known as the Blandford-Znajek mechanism, to extract rotation energy by using the interaction between a rotating black hole and its surrounding electromagnetic field, successfully explaining the phenomenon of AGN jets [16]. Therefore, the Blandford-Znajek mechanism is now regarded as the primary mechanism responsible for powering the relativistic jets of AGN. Later, Koide and Arai suggested that magnetic reconnection in the ergospheric plasma could provide an alternative energy extraction channel [17], while Comisso and Asenjo performed a detailed study on extracting energy from Kerr black holes via magnetic reconnection [18]. The work of Comisso and Asenjo indic-

Received 12 December 2025; Accepted 26 January 2026; Accepted manuscript online 27 January 2026

* Supported by the National Natural Science Foundation of China (12475055, 12247101), the Basic Research Foundation of Central Universities (lzujbky-2024-jdzx06), the Natural Science Foundation of Gansu Province (22JR5RA389) and the `111 Center' (B20063)

† E-mail: weishw@lzu.edu.cn (Corresponding author)

ated that, under specific plasma conditions, magnetic reconnection processes might surpass the Blandford-Znajek mechanism in energy extraction efficiency [18]. Moreover, the detection of magnetic fields around the supermassive black hole M87* at its center [19, 20] confirms the existence of magnetic fields in the vicinity of a real black hole. This further demonstrates the feasibility of the magnetic reconnection mechanism for energy extraction. Thus, in this paper, we explore energy extraction based on the work of Comisso and Asenjo.

The mechanism of energy extraction from a black hole via magnetic reconnection can be described as follows. In the case of a rapidly rotating black hole embedded in a magnetic field, the frame-dragging effect induces the formation of an anti-parallel magnetic field configuration in the equatorial plane [21−24]. This configuration gives rise to a current sheet, which is inherently unstable. When the size of the current sheet exceeds the critical aspect ratio [25−27], it will be destroyed by the instability of the plasma and cause the magnetic field lines with opposite directions on both sides of the current sheet to be close to each other, cutting off and rapidly reconnecting, and then forming two new magnetic field lines [28−31]. Because the two new magnetic field lines are highly curved, the magnetic tension is large. Consequently, part of the plasma accelerates under the intense magnetic tension, while another part decelerates. The accelerated particles gain more kinetic energy and escape to infinity, while the decelerated particles move towards the black hole, ultimately being captured by it. To the observer at infinity, the decelerated particles have negative energy and their absorption by the black hole effectively diminishes the black hole's total energy, while the escaping jet component carries away rotational energy [17, 18, 32, 33]. As the plasma moves out of the reconnection region, the magnetic tension relaxes, and the magnetic field lines deform again under the frame-dragging effect, triggering rapid magnetic reconnection [17, 18, 28] and repeating the energy extraction process. The dominant reconnection radial location of magnetic reconnection is called the X-point, which lies within the ergosphere of a rotating black hole.

In recent years, the mechanism of energy extraction via magnetic reconnection has been significantly expanded. For instance, this mechanism has been applied to more black holes for research on black hole energy extraction, such as Lorentz breaking Kerr-Sen and Kiselev black holes [34], the spinning braneworld black hole [32], Kerr-MOG black holes [35], rotating hairy black holes [36], Konoplya-Rezzolla-Zhidenko parametrized black holes [37], and others [38−45]. Analyses have also been proposed concerning energy extraction through magnetic reconnection processes in the plunging region of black holes [46−52]. These studies demonstrate that black hole parameters, such as the Lorentz breaking parameter, tidal charge, modified gravity parameter, hairy parameters, and deformation parameters, along with properties of the plunging region, significantly influence the efficiency of energy extraction via magnetic reconnection. Such progress has stimulated further exploration of both gravitational theories and mechanisms for extracting energy from black holes.

Meanwhile, research on AdS spacetime continues to be a topic of significant interest. AdS spacetime is a solution to Einstein's field equations with a negative cosmological constant ($\Lambda < 0$), characterized by unique geometric structures and physical properties [53]. It plays a crucial role in gravitational theory and related areas of theoretical physics. The AdS/CFT correspondence, proposed by Maldacena [54], establishes a duality between gravitational theories in AdS spacetime and conformal field theories (CFT) on its boundary. This correspondence has advanced the study of black hole thermodynamics and the holographic principle. The holographic nature of AdS spacetime suggests that a gravitational theory in a higher-dimensional AdS spacetime can be equivalently described by a lower-dimensional CFT, providing a crucial tool for studying quantum gravitational effects [55−58]. In AdS space, a phase transition from a stable large Schwarzschild black hole to a thermal gas space is known as the Hawking-Page transition [59, 60]. According to the AdS/CFT correspondence, this phase transition is interpreted as the confinement/deconfinement phase transition. In AdS spacetime, the cosmological constant is regarded as the thermodynamic pressure, and rich phase transitions are uncovered [61−65]. In particular, the energy extraction via magnetic reconnection in Kerr-de Sitter ($\Lambda > 0$) spacetime was investigated in Ref. [33]. It was found that as the positive cosmological constant increases, a slowly rotating Kerr-de Sitter black hole can achieve energy extraction more efficiently than a Kerr black hole. Considering that the negative cosmological constant [66] makes its spacetime structure significantly different from that of Kerr black holes and Kerr-de Sitter black holes, in this study, we attempt to investigate energy extraction via the magnetic reconnection in the background of a Kerr-AdS black hole.

The remainder of this paper is organized as follows. In Sec. II, we introduce the Kerr-AdS black hole spacetime and analyze the geodesic motion of photons in its vicinity, from which several characteristic orbit radii will be derived. In Sec. III, we calculate the hydrodynamic energy-at-infinity per unit enthalpy of the surrounding plasma for the Kerr-AdS black hole and determine the condition for energy extraction. Section IV is devoted to examining the parameter space within which energy extraction is viable. In Sec. V, we investigate the efficiency and power of energy extraction from Kerr-AdS black holes. Finally, we summarize the key results of this study in Sec. VI.

II. KERR-ADS BLACK HOLE AND GEODESICS OF PHOTONS

The metric of the Kerr-AdS black hole that we will discuss can be written in Boyer-Lindquist coordinates (t, r, θ, ϕ) as (taking the geometrized units with $G = c = 1$) [66]

$$\begin{aligned} \mathrm{d}s^2 = &-\frac{\Delta_r - \Delta_\theta a^2 \sin^2\theta}{\rho^2}\mathrm{d}t^2 + \frac{\rho^2}{\Delta_r}\mathrm{d}r^2 + \frac{\rho^2}{\Delta_\theta}\mathrm{d}\theta^2 \\ &+ \frac{\sin^2\theta}{\Sigma^2\rho^2}[(r^2+a^2)^2\Delta_\theta - \Delta_r a^2\sin^2\theta]\mathrm{d}\phi^2 \\ &+ \frac{2a\sin^2\theta}{\Sigma^2\rho^2}[(r^2+a^2)^2\Delta_\theta - \Delta_r]\mathrm{d}t\mathrm{d}\phi, \end{aligned} \tag{1}$$

where the metric functions are given by

$$\Delta_r = (r^2+a^2)\left(1-\frac{\Lambda r^2}{3}\right) - 2Mr, \tag{2}$$

$$\Delta_\theta = 1 + \frac{\Lambda}{3}a^2\cos^2\theta, \tag{3}$$

$$\rho^2 = r^2 + a^2\cos^2\theta, \tag{4}$$

$$\Sigma = 1 + \frac{\Lambda a^2}{3}. \tag{5}$$

Parameters M and a denote the mass and spin of the black hole, respectively. For the Kerr-AdS black, the cosmological constant Λ takes negative values. For $\Lambda = 0$, the metric (1) reduces to the standard Kerr metric.

Because the energy extraction of the mechanism we considered occurs within the region bounded by the outer horizon and the outer infinite redshift surface, known as the ergosphere, we focus on determining the outer event horizon radius and outer infinite redshift surface radius of Kerr-AdS black holes.

The location of the Kerr black hole's event horizon is given by the solution of the equation $\Delta_r = 0$. This is a quartic equation for r with two positive and two negative roots. The negative roots do not have physical significance, while the two positive roots represent the inner event horizon radius r_- and outer event horizon radius r_+ of the black hole, with $r_+ \geq r_-$. Both r_- and r_+ depend on the black hole mass M, spin parameter a, and cosmological constant Λ. Due to the complexity and length of their explicit analytical expressions, we resort to numerical methods for subsequent analysis. By solving the inequality $r_+ \geq r_-$, we determine the parameter space of $\Lambda M^2 - a/M$ that allows the existence of Kerr-AdS black holes, as illustrated in Fig. 1. In this figure, the region shaded in blue corresponds to parameter values for which Kerr-AdS black holes can exist. The solid blue curve indicates the condition $r_+ = r_-$, at which the inner and outer event horizons coincide and the black holes become extremal. Moreover, we observe that as $a/M \to 1$, ΛM^2 approaches zero, whereas as $a/M \to 1$, ΛM^2 can decrease without bound, tending toward negative infinity. Figure 1 shows the part of the parameter space where ΛM^2 ranges from −50 to 0.

The position of the outer boundary of the ergosphere, *i.e.*, the outer infinite redshift surface, can be given by the following equation:

$$g_{tt} = -\frac{\Delta_r - \Delta_\theta a^2\sin^2\theta}{\rho^2} = 0. \tag{6}$$

In this paper, considering that the plasma undergoing magnetic reconnection moves in the equatorial plane, hereinafter, $\theta = \frac{\pi}{2}$ is assumed. It can be solved that the position of the outer ergosphere's boundary r_{E} is

$$\begin{aligned} r_{\mathrm{E}} = &\frac{-3 + a^2\Lambda}{(81M\Lambda^2 + 3\sqrt{3}\sqrt{\Lambda^3(243M^2\Lambda + (-3+a^2\Lambda)^3)})^{1/3}} \\ &- \frac{(27M\Lambda^2 + \sqrt{3}\sqrt{\Lambda^3(243M^2\Lambda + (-3+a^2\Lambda)^3)})^{1/3}}{3^{2/3}\Lambda}. \end{aligned} \tag{7}$$

As the plasma orbiting a black hole in the equatorial plane cannot reside at radii smaller than the light ring, we investigate the geodesic motion of photons in the Kerr-AdS black hole spacetime. According to the Hamilton-Jacobi equation, the geodesics of photons in this background are governed by the following expression [67−69]:

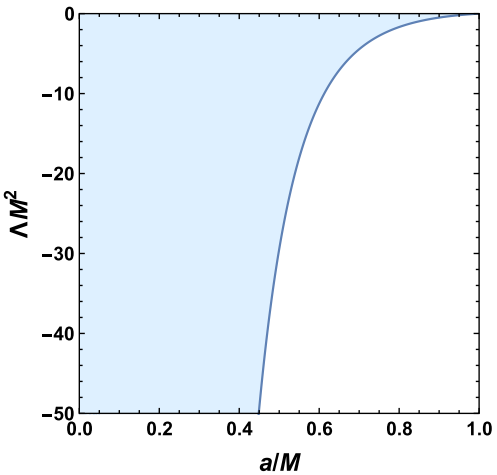

Fig. 1. (color online) Parameter space allowing the existence of Kerr-AdS black holes in $a/M - \Lambda M^2$ plane (shaded region). The solid line denotes extremal Kerr-AdS black holes.

$$\frac{\mathrm{d}r}{\mathrm{d}\lambda}=\frac{\sqrt{U(r)}}{\rho^2}, \tag{8}$$

$$\frac{\mathrm{d}\theta}{\mathrm{d}\lambda}=\frac{\sqrt{U(\theta)}}{\rho^2}, \tag{9}$$

$$\frac{\mathrm{d}\phi}{\mathrm{d}\lambda}=\frac{a\Sigma(a^2\sin^2\theta+\rho^2)-aL\Sigma}{\rho^2\Delta_r}+\frac{L\Sigma^2-a\Sigma E\sin^2}{\rho^2\Delta_\theta\sin^2}, \tag{10}$$

$$\frac{\mathrm{d}t}{\mathrm{d}\lambda}=\frac{(a^2\sin^2\theta+\rho^2)(a^2E\sin^2\theta-aL\Sigma+E\rho^2)}{\rho^2\Delta_r}+\frac{a(L\Sigma-aE\sin^2\theta)}{\rho^2\Delta_\theta}, \tag{11}$$

where L, E, λ, and K are the energy, angular momentum, affine parameter, and Carter constant [66], respectively. $U(r)=[E(a^2\sin^2\theta+\rho^2)-aL\Sigma]^2-\Delta_r[(L\Sigma-aE)^2+K]$ and $U(\theta)=\Delta_\theta[(L\Sigma-aE)^2+K]-(L\Sigma\csc\theta-aE\sin\theta)^2$ are non-negative definite functions of r and θ, respectively. A photon along the circular orbit in the equatorial plane should satisfy the following conditions:

$$U(r_{\mathrm{LR}})=0, \qquad \frac{\mathrm{d}U(r_{LR})}{\mathrm{d}r}=0. \tag{12}$$

Solving the above equation could yield the corotating orbital radius of the photon around the black hole, which we demonstrate to depend functionally on the mass M, spin a, and cosmological constant Λ. Because the analytical expression is more complex, we employ numerical methods to investigate the orbit characteristics.

We plot the radii of the outer event horizon r_+ (red solid curves), outer ergosphere boundary r_{E} (black solid curves), and circular corotating photon orbit r_{LR} (purple dashed curves) as a function of the cosmological constant ΛM^2 for a fixed spin parameter $a/M=0.99$ in Fig. 2(a) and as functions of the spin parameter a/M for a fixed cosmological constant $\Lambda M^2=-0.01$ in Fig. 2(b). In Fig. 2(a), for a fixed a/M, all these three radii increase monotonically with ΛM^2. Significantly, the circular corotating photon orbit is located very close to the outer event horizon under these conditions. Moreover, the outer ergosphere boundary consistently extends beyond both the outer horizon and circular photon orbit. When ΛM^2 reaches its minimum value, the black hole approaches the extremal limit, and the circular photon orbit coincides precisely with the outer event horizon. Fig. 2(b) demonstrates that, for a fixed ΛM^2, all these three radii decrease as the spin parameter a/M increases. When a/M is small, the outer ergosphere boundary lies very close to the event horizon, and the black hole begins to resemble the Schwarzschild solution, with the ergosphere becoming increasingly narrow. As a/M approaches its maximum value, the black hole becomes extremal, and again, the circular corotating photon orbit coincides with the outer horizon.

III. ENERGY EXTRACTION VIA MAGNETIC RECONNECTION

In this section, we calculate the hydrodynamic energy-at-infinity per enthalpy of the plasma $\epsilon_{\pm}^{\infty}$ surrounding the Kerr-AdS black hole and analyze the condition for energy extraction.

To analyze the plasma energy density conveniently, we adopt the zero-angular-momentum-observer (ZAMO) frame [70–71], where the line element of spacetime is written in the following form:

$$\mathrm{d}s^2=\eta_{\mu\nu}\mathrm{d}\hat{x}^\mu\mathrm{d}\hat{x}^\nu=-\mathrm{d}\hat{t}^2+\Sigma_{i=1}^{3}(\mathrm{d}\hat{x}^i)^2. \tag{13}$$

The coordinate transformation between the Boyer-Lindquist frame and ZAMO frame is

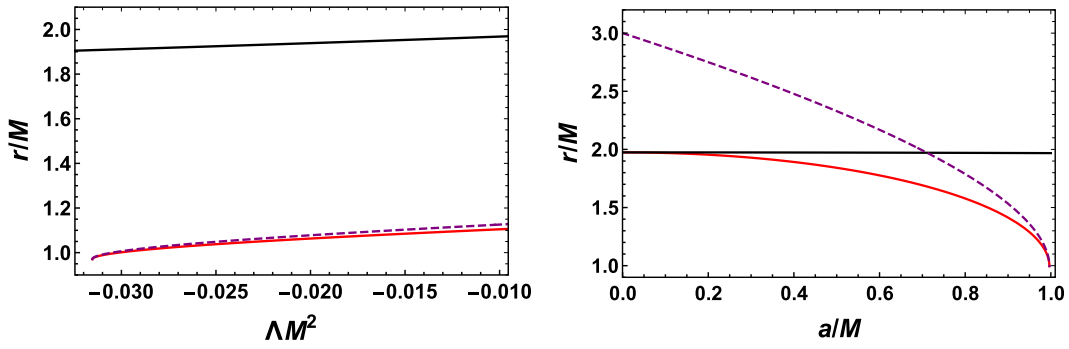

(a) $a/M=0.99$ (b) $\Lambda M^2=-0.01$

Fig. 2. (color online) Characteristic radii for black holes. The outer event horizon r_+, outer ergosphere boundary r_{E}, and circular corotating photon orbit r_{LR} are described by the red solid curves, black solid curves, and purple dashed curves, respectively. (a) r/M vs. ΛM^2. (b) r/M vs. a/M.

$$\mathrm{d}\hat{t} = \alpha \mathrm{d}t, \quad \mathrm{d}\hat{x}^i = \sqrt{g_{ii}}\mathrm{d}x^i - \alpha\beta^i \mathrm{d}t, \tag{14}$$

where the lapse function α and shift vector $\beta^i = (0,0,\beta^\phi)$ can be expressed as

$$\alpha = \sqrt{-g_{tt} + \frac{g_{t\phi}^2}{g_{\phi\phi}}}, \quad \beta^\phi = \sqrt{g_{\phi\phi}}\frac{\omega^\phi}{\alpha}, \tag{15}$$

with $\omega^\phi = -g_{t\phi}/g_{\phi\phi}$ being the angular velocity of the frame dragging.

For the contravariant components a^μ and covariant components a_μ of a vector in the Boyer-Lindquist frame, the corresponding relationships when transforming to the ZAMO frame are as follows:

$$\hat{a}^0 = \alpha a^0, \qquad \hat{a}^i = \sqrt{g_{ii}}a^i - \alpha\beta^i a^0, \tag{16}$$

$$\hat{a}_0 = a_0/\alpha + \Sigma_{i=1}^3(\beta^i/g_{ii})a_i, \qquad \hat{a}_i = a_i/\sqrt{g_{ii}}. \tag{17}$$

Next, we analyze the energy density of the plasma. In the one-fluid approximation, the energy-momentum tensor for the plasma can be written as [17–18, 72–73]

$$T^{\mu\nu} = pg^{\mu\nu} + \omega U^\mu U^\nu + F^\mu_\sigma F^{\nu\sigma} - \frac{1}{4}g^{\mu\nu}F^{\rho\sigma}F_{\rho\sigma}, \tag{18}$$

where p, ω, U^μ, and $F^{\mu\nu}$ are the proper plasma pressure, enthalpy density, four-velocity, and electromagnetic field tensor, respectively. The energy-at-infinity density is defined as follows [17, 18]:

$$e^\infty = -\alpha g_{\mu 0}T^{\mu 0} = \alpha\hat{e} + \alpha\beta^\phi\hat{P}^\phi. \tag{19}$$

The total energy density $\hat{e}$ and azimuthal component of the momentum density $\hat{P}^\phi$ are

$$\begin{aligned}\hat{e} &= \omega\hat{\gamma}^2 - p + \frac{1}{2}(\hat{B}^2 + \hat{E}^2),\\ \hat{P}^\phi &= \omega\hat{\gamma}^2\hat{v}^\phi + (\hat{B}\times\hat{E})^\phi,\end{aligned} \tag{20}$$

where $\hat{\gamma} = \hat{U}^0 = \sqrt{1-\Sigma_{i=1}^3(\mathrm{d}\hat{v}^i)^2}$, $\hat{B}^i = \epsilon^{ijk}F_{jk}/2$, and $\hat{E}^i = \eta^{ij}\hat{F}_{j0} = \hat{F}_{i0}$ [18, 74–75] represent the Lorentz factor and components of the magnetic and electric fields, respectively. $\hat{v}^\phi$ is the outflow velocity component of the plasma after magnetic reconnection in the ZAMO frame.

The energy-at-infinity density e^∞ can be divided into two parts: hydrodynamic component e^∞_{hyd} and electromagnetic component e^∞_{em}. Thus, we can obtain $e^\infty = e^\infty_{\mathrm{hyd}} + e^\infty_{\mathrm{em}}$ with [18]

$$\begin{aligned}e^\infty_{\mathrm{hyd}} &= \alpha(\omega\hat{\gamma}^2 - p) + \alpha\beta^\phi\omega\hat{\gamma}^2\hat{v}^\phi,\\ e^\infty_{\mathrm{em}} &= \alpha(\hat{B}^2 + \hat{E}^2)/2 + \alpha\beta^\phi(\hat{B}\times\hat{E})_\phi.\end{aligned} \tag{21}$$

It is considered that magnetic reconnection is a very efficient process, which converts most of the magnetic energy into the kinetic energy of the plasma, so the electromagnetic energy-at-infinity density will be insignificant. Therefore, considering the condition that the plasma is incompressible and adiabatic, the energy-at-infinity density of the plasma can be written as

$$e^\infty = e^\infty_{\mathrm{hyd}} = \alpha\left((\hat{\gamma} + \beta^\phi\hat{\gamma}\hat{v}^\phi)\omega - \frac{p}{\hat{\gamma}}\right). \tag{22}$$

To study the localized magnetic reconnection process, the local rest frame $x'^\mu = (x'^0, x'^1, x'^2, x'^3)$, in which x'^1 is parallel to the direction of $x^1 = r$ and x'^3 is parallel to the direction of $x^3 = \phi$, is employed. In the Boyer-Lindquist coordinate system, this local rest frame moves with the plasma corotating around the Kerr-AdS black hole in the circular orbit within the equatorial plane with the Kepler angular velocity Ω_{K}, which can be given by the following equation:

$$\Omega_{\mathrm{K}} = \frac{\mathrm{d}\phi}{\mathrm{d}t} = \frac{-g_{t\phi,r} + \sqrt{g_{t\phi,r}^2 - g_{tt,r}g_{\phi\phi,r}}}{g_{\phi\phi,r}} = \frac{\sqrt{M - \frac{1}{3}r^3\Lambda}}{a\sqrt{M - \frac{1}{3}r^3\Lambda} + r^{3/2}}. \tag{23}$$

In the ZAMO frame, the Keplerian angular velocity can be expressed as

$$\hat{v}_{\mathrm{K}} = \frac{\mathrm{d}\hat{\phi}}{\mathrm{d}\hat{t}} = \frac{\mathrm{d}\hat{\phi}/\mathrm{d}\lambda}{\mathrm{d}\hat{t}/\mathrm{d}\lambda} = \frac{g_{\phi\phi}\mathrm{d}x^\phi/\mathrm{d}\lambda - \alpha\beta^\phi\mathrm{d}t/\mathrm{d}\lambda}{\alpha\mathrm{d}t/\mathrm{d}\lambda} = \frac{\Omega_{\mathrm{K}}\sqrt{g_{\phi\phi}}}{\alpha} - \beta^\phi. \tag{24}$$

Then, the plasma outflow velocity in the local rest frame is expressed by v'_{out}, which is related to the plasma magnetization and can be expressed as [18]

$$v'_{\mathrm{out}} = \sqrt{\frac{\sigma_0}{1+\sigma_0}}. \tag{25}$$

Here, $\sigma_0 = B_0^2/\omega_0$ is the plasma magnetization upstream of the reconnection layer and B_0 is the asymptotic macro-scale magnetic field. The azimuthal component of the plasma outflow velocity can be written in the ZAMO frame as follows [18]:

$$\hat{v}^\phi_\pm = \frac{\hat{v}_{\mathrm{K}} \pm v'_{\mathrm{out}}\cos\xi}{1 \pm \hat{v}_{\mathrm{K}}v'_{\mathrm{out}}\cos\xi}, \tag{26}$$

where "+" and "-" represent the accelerating and decelerating parts of the plasma, respectively. In addition, $\xi = \arctan(v'^{1}_{\rm out}/v'^{3}_{\rm out})$ is the plasma orientation angle. $v'^{1}_{\rm out}$ and $v'^{3}_{\rm out}$ denote the radial and azimuthal components of plasma velocities in the local rest frame, respectively.

Then, by introducing the Lorentz factor $\hat{\gamma}_{\rm K} = 1/\sqrt{1-\hat{v}^2_{\rm K}}$, the plasma energy-at-infinity density per enthalpy is [18]

$$\begin{aligned}\epsilon^{\infty}_{\pm} &= e^{\infty}_{\rm hyd\pm}/\omega \\ &= \alpha\hat{\gamma}_{\rm K}((1+\beta^{\phi}\hat{v}_{\rm K})\sqrt{1+\sigma_0} \pm \cos\xi(\beta^{\phi}+\hat{v}_{\rm K})\sqrt{\sigma_0} \\ &\quad - \frac{\sqrt{1+\sigma_0} \mp \cos\xi\hat{v}_{\rm K}\sqrt{\sigma_0}}{4\hat{\gamma}^2_{\rm K}(1+\sigma_0-\cos^2\xi\hat{v}^2_{\rm K}\sigma_0)}),\end{aligned} \tag{27}$$

where we have assumed that the plasma is relativistic hot, so $p = \omega/4$ [18] is used. To achieve energy extraction, the requirements for the energy densities $\epsilon^{\infty}_{\pm}$ of decelerating and accelerating particles are

$$\epsilon^{\infty}_{-} < 0, \qquad \Delta\epsilon^{\infty}_{+} = \epsilon^{\infty}_{+} - (1 - \frac{\Gamma}{\Gamma-1}\frac{p}{\omega}) = \epsilon^{\infty}_{+} > 0, \tag{28}$$

for relativistically hot plasma with polytropic index $\Gamma = 4/3$ [18]. If the decelerating plasma acquires negative energy measured at infinity, the accelerating plasma shall gain kinetic energy greater than its original energy at infinity. As a result, the rotational energy of the black hole is extracted.

It can be seen from Eq. (28) that the energy-at-infinity per enthalpy of the plasma $\epsilon^{\infty}_{\pm}$ is a function of the black hole spin a, cosmological constant Λ, black hole mass M, magnetization of plasma σ_0, orientation angle of plasma outflow velocity ξ, and dominant reconnection radial location r. To investigate how these quantities affect energy extraction, we plot ϵ^{∞}_{+} and ϵ^{∞}_{-} in Fig. 3 and Fig. 4, respectively.

In Fig. 3, we plot $\epsilon^{\infty}_{\pm}$ as functions of the spin parameter a/M for varying values of the plasma magnetization σ_0, orientation angle ξ, and dominant reconnection radial location r/M, with the cosmological constant fixed at $\Lambda M^2 = -0.01$. From Figs. 3(a), 3(c), 3(e), and 3(g), it can be seen that ϵ^{+}_{∞} remains strictly positive across all parameter variations. However, from Figs. 3(b), 3(d), 3(f), and 3(h), one can see that ϵ^{-}_{∞} is negative when the black hole spin is beyond some certain values, which indicates that the conditions of (28) are satisfied, and energy extraction is possible. In particular, ϵ^{∞}_{-} decreases with the spin a/M, which implies that more energy can be extracted for a larger spin.

As the plasma magnetization σ_0 increases from 5 to 20, with all other parameters held fixed, ϵ^{∞}_{-} decreases, indicating that greater plasma magnetization leads to enhanced extraction of rotational energy from the black hole. A high degree of plasma magnetization implies the presence of a strong magnetic field configuration around the black hole, in which magnetic reconnection facilitates a more efficient conversion of stored magnetic energy into plasma kinetic energy, thereby enabling increased energy extraction from the black hole. A comparative analysis of Figs. 3(d) and 3(h), conducted under fixed parameters, namely, a dominant reconnection radial location of $r/M = 1.15$, identical black hole spin, and consistent plasma magnetization, reveals that reducing the magnetic orientation angle ξ from $\frac{\pi}{6}$ to $\frac{\pi}{12}$ results in lower ϵ^{∞}_{-}. This behavior signifies an increase in the amount of energy extracted from the black hole. These results show notable qualitative agreement with the conclusions drawn in Ref. [18], which investigated the influence of the Kerr black hole's and plasma's physical parameters on energy extraction. Furthermore, in Figs. 3(b), 3(d), and 3(f), we fix the magnetic orientation angle at $\xi = \frac{\pi}{12}$ while maintaining constant values for the black hole spin and plasma magnetization and sequentially vary the dominant reconnection radial location as $r/M = 1.1$, $r/M = 1.4$, and $r/M = 1.6$. In these cases, the value of ϵ^{+}_{∞} increases as r/M increases.

We now turn to explore the dependence of the cosmological constant by plotting $\epsilon^{\infty}_{\pm}$ against ΛM^2 for $a/M = 0.99$ and varying σ_0, ξ, r/M in Fig. 4. In Figs. 4(a), 4(c), 4(e), and 4(g), ϵ^{∞}_{+} consistently remains above 0. Therefore, our focus lies solely on ϵ^{∞}_{-}, depicted in Figs. 4(b), 4(d), 4(f), and 4(h). Notably, in Figs. 4(b) and 4(h), with the dominant reconnection radial location set at $r/M = 1.15$ and orientation angles $\xi = \frac{\pi}{6}$ and $\frac{\pi}{12}$, respectively, the results are consistent with the behaviors observed in Fig. 3, indicating that smaller values of ξ lead to lower values of ϵ^{∞}_{-}. Similarly, we can draw a parallel to Fig. 3 by concluding that an increase in plasma magnetization corresponds to a decrease in ϵ^{∞}_{-}. However, unlike that observed in Fig. 3, the comparison in subplots Fig. 4(b), 4(d), 4(f), and 4(i) reveals that ϵ^{∞}_{-} does not exhibit a consistent monotonic increase or decrease with the rise in ΛM^2 at the dominant reconnection radial location r/M. For example, in Fig. 4(b), with $r/M = 1.15$ and $\xi = \frac{\pi}{12}$, ϵ^{∞}_{-} demonstrates a continuous increase with ΛM^2. Contrastingly, in Figs. 4(d) and 4(i) (where Fig. 4(i) offers a clearer representation of the behavior of ϵ^{∞}_{-} when σ_0 is set to 5 in Fig. 4(d)) with $r/M = 1.35$ and $\xi = \frac{\pi}{12}$, a distinct behavior is observed where ϵ^{∞}_{-} initially decreases and then increases with increasing ΛM^2. In Fig. 4(f) with $r/M = 1.75$ and $\xi = \frac{\pi}{12}$, ϵ^{∞}_{-} decreases as ΛM^2 increases. This illustrates that the impact of the cosmological constant on energy extraction is influenced by the specific dominant reconnection radial location.

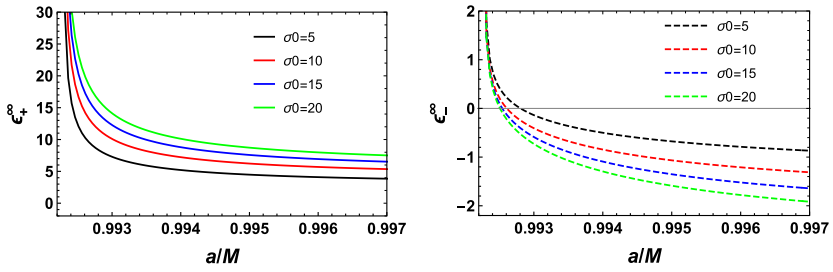

(a) $r/M = 1.1, \xi = \pi/12$ (b) $r/M = 1.1, \xi = \pi/12$

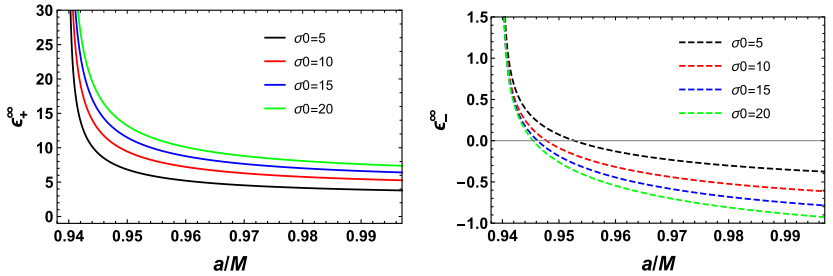

(c) $r/M = 1.4, \xi = \pi/12$ (d) $r/M = 1.4, \xi = \pi/12$

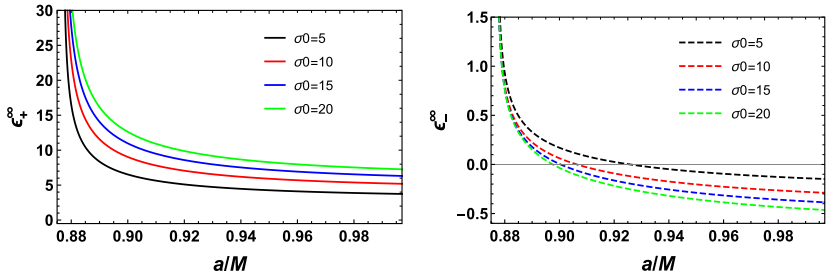

(e) $r/M = 1.6, \xi = \pi/12$ (f) $r/M = 1.6, \xi = \pi/12$

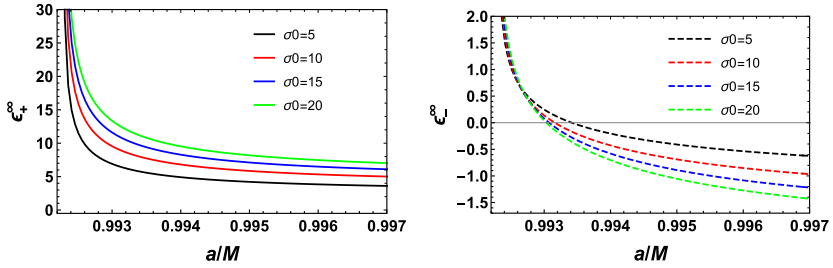

(g) $r/M = 1.1, \xi = \pi/6$ (h) $r/M = 1.1, \xi = \pi/6$

Fig. 3. (color online) Behaviors of ϵ_+^∞ (solid curves) and ϵ_-^∞ (dashed curves) as functions of spin a/M for different values of the plasma magnetization σ_0, orientation angle ξ, and dominant reconnection radial location r/M and with cosmological constant $\Lambda M^2 = -0.01$ fixed. The plasma magnetization σ_0 = 5, 10, 15, and 20 goes from bottom to top for solid curves and from top to bottom for dashed curves.

IV. PARAMETER SPACES FOR ENERGY EXTRACTION

In the preceding section, we calculated the hydrodynamic energy-at-infinity per enthalpy of the plasma, denoted as $\epsilon_\pm^\infty$, and the energy extraction condition outlined in (28) through the magnetic reconnection mechanism. Obviously, the value of ϵ_+^∞ consistently remains positive. As a result, our primary focus concerning the energy extraction condition centers on ensuring $\epsilon_-^\infty < 0$.

This section examines the parameter space. In Fig. 5 and Fig. 6, we present the regions within the parameter spaces of $\Lambda M^2 - r/M$ and $a/M - \Lambda M^2$, respectively. These regions exhibit the configurations that satisfy the energy

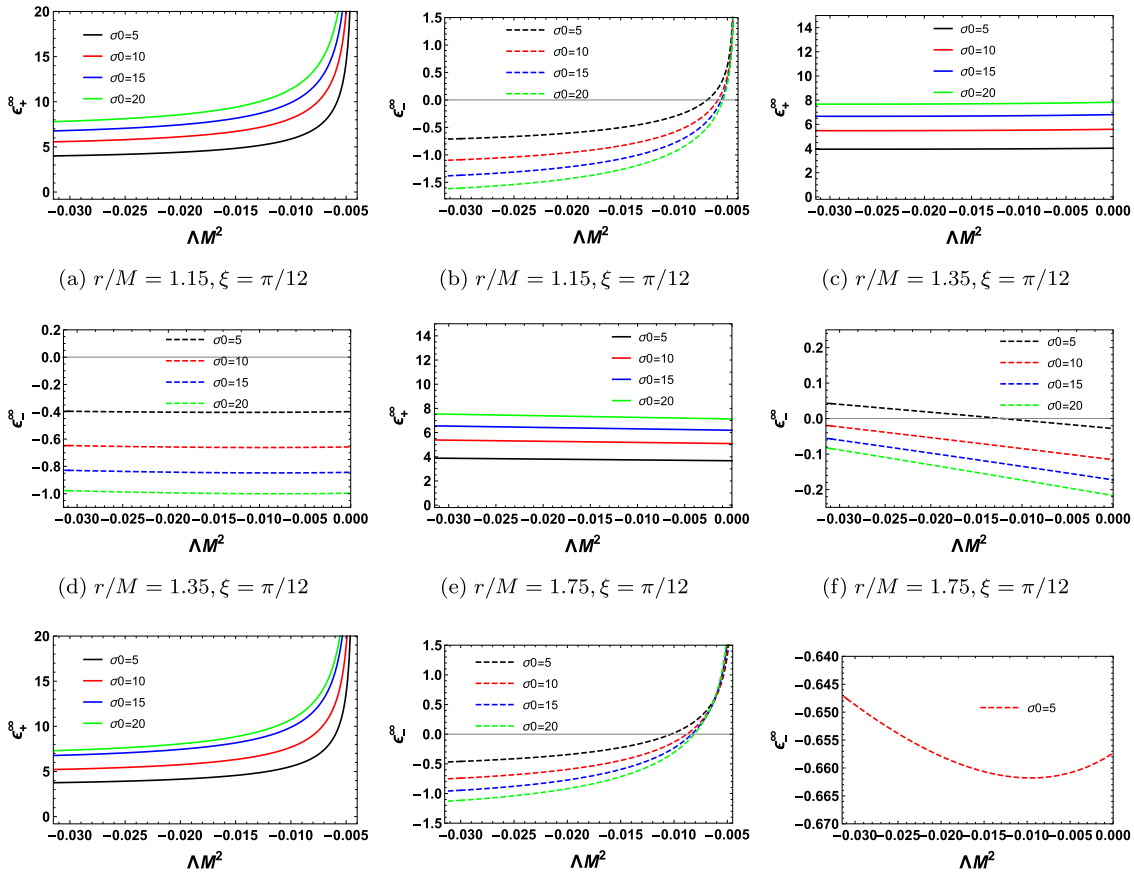

(a) $r/M = 1.15, \xi = \pi/12$ (b) $r/M = 1.15, \xi = \pi/12$ (c) $r/M = 1.35, \xi = \pi/12$

(d) $r/M = 1.35, \xi = \pi/12$ (e) $r/M = 1.75, \xi = \pi/12$ (f) $r/M = 1.75, \xi = \pi/12$

(g) $r/M = 1.15, \xi = \pi/6$ (h) $r/M = 1.15, \xi = \pi/6$ (i) $r/M = 1.35, \xi = \pi/12$

Fig. 4. (color online) Behaviors of ϵ_+^∞ (solid curves) and ϵ_-^∞ (dashed curves) as functions of the cosmological constant ΛM^2 for different values of the plasma magnetization of plasma σ_0, the orientation angle ξ, and the dominant reconnection radial location r/M, and with spin $a/M = 0.99$ fixed. The plasma magnetization σ_0 = 5, 10, 15, and 20 from bottom to top for solid curves and from top to bottom for dashed curves. (a) $r/M = 1.15$, $\xi = \pi/12$. (b) $r/M = 1.15$, $\xi = \pi/12$. (c) $r/M = 1.35$, $\xi = \pi/12$. (d) $r/M = 1.35$, $\xi = \pi/12$. (e) $r/M = 1.75$, $\xi = \pi/12$. (f) $r/M = 1.75$, $\xi = \pi/12$. (g) $r/M = 1.15$, $\xi = \pi/6$. (h) $r/M = 1.15$, $\xi = \pi/6$. (i) $r/M = 1.35$, $\xi = \pi/12$. (i) shows the behavior of ϵ_-^∞ when σ_0 is set to 5 in (d).

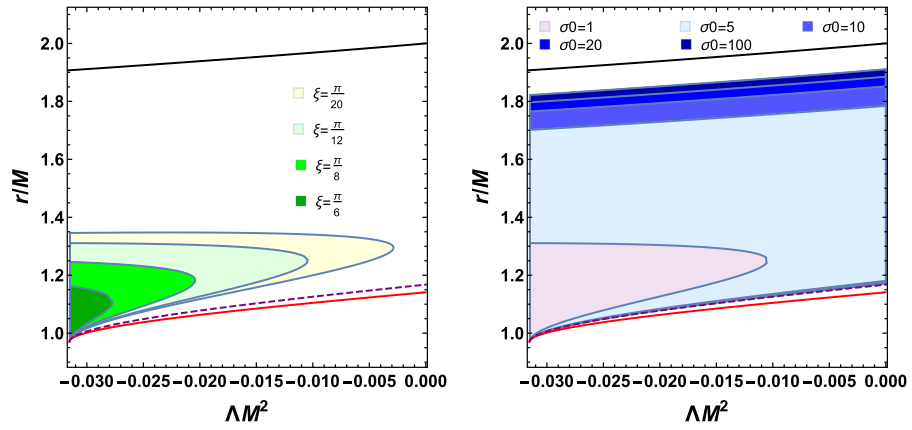

(a) $\sigma_0 = 1$ (b) $\xi = \frac{\pi}{12}$

Fig. 5. (color online) Regions of parameter space $\Lambda M^2 - r/M$ satisfying the energy extraction condition $\epsilon_-^\infty < 0$ with $a/M = 0.99$. Red solid curves, black solid curves, and purple dashed curves represent the radii of the outer event horizon r_+, outer ergosphere boundary $r_{\rm E}$, and circular corotating photon orbit $r_{\rm LR}$, respectively. (a) $\sigma_0 = 1$ with $\xi = \frac{\pi}{6}, \frac{\pi}{8}, \frac{\pi}{12}, \frac{\pi}{20}$. (b) $\xi = \frac{\pi}{12}$ with σ_0=1, 5, 10, 20, 100.

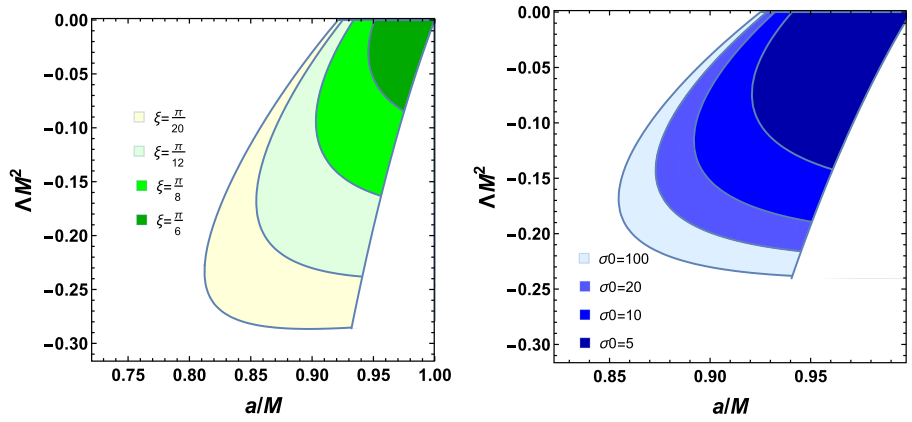

(a) $\sigma_0 = 1$ (b) $\xi = \frac{\pi}{12}$

Fig. 6. (color online) Regions of parameter space $a/M - \Lambda M^2$ satisfying the energy extraction condition $\epsilon_{-}^{\infty} < 0$ with $a/M = 0.99$. The right boundaries of the shaded regions in both subplots correspond to the relationship curves between a/M and ΛM^2 when the Kerr-AdS black hole is an extremal black hole. (a) $\sigma_0 = 1$ with $\xi = \frac{\pi}{6}, \frac{\pi}{8}, \frac{\pi}{12}, \frac{\pi}{20}$. (b) $\xi = \frac{\pi}{12}$ with σ_0=1, 5, 10, 20, 100.

extraction condition $\epsilon_{-}^{\infty} < 0$, offering a visual representation of how the cosmological constant influences the permissible range of physical parameters for energy extraction.

First, in Fig. 5, we delineate the regions in the parameter space of $\Lambda M^2 - r/M$ that satisfy the energy extraction condition $\epsilon_{\pm}^{\infty} < 0$ for a rapidly rotating black hole with $a/M = 0.99$. Moving to Fig. 5(a), we explore the impact of the orientation angle ξ under a constant plasma magnetization of $\sigma_0 = 1$. Shaded regions highlight negative values of $\epsilon_{\pm}^{\infty}$ for different ξ values, such as $\frac{\pi}{6}$, $\frac{\pi}{8}$, $\frac{\pi}{12}$, and $\frac{\pi}{20}$. Fig. 5(b) delves into the influence of various plasma magnetization levels ($\sigma_0 = 1$, 5, 10, 20, and 100) while maintaining a fixed orientation angle of $\xi = \frac{\pi}{12}$. This analysis reveals similar energy extraction parameter spaces across different magnetization values. Within the two subplots of Fig. 5, the red solid curves, black solid curves, and purple dashed curves correspond to the radii of the outer event horizon r_+, outer ergosphere boundary $r_{\rm E}$, and circular corotating photon orbit $r_{\rm LR}$, respectively, as depicted in Fig. 2(a). The shaded areas between $r_{\rm E}$ and $r_{\rm LR}$ signify the occurrence of magnetic reconnection within the ergosphere but beyond the photon orbit. Decreasing ξ or increasing σ_0 expands these regions, broadening the permissible ranges of the parameter space in terms of ΛM^2 and r/M for energy extraction. Importantly, the introduction of a negative cosmological constant systematically widens the acceptable range of the dominant reconnection radial location r/M that complies with the energy extraction condition. This range consistently increases as the value of ΛM^2 decreases. Consequently, we infer that Kerr-AdS black holes facilitate energy extraction by plasmas across a broader radial spectrum for reconnection locations compared to their Kerr counterparts.

Subsequently, in Fig. 6, we show the $a/M - \Lambda M^2$ parameter space to identify regions where $\epsilon_{\pm}^{\infty} < 0$ while maintaining a fixed $r/M = 1.5$. Moving to Fig. 6(a), we present the outcomes for plasma magnetization at $\sigma_0 = 100$. Shaded regions denote negative values of $\epsilon_{\pm}^{\infty}$ corresponding to various orientation angles, such as $\xi = \frac{\pi}{6}, \frac{\pi}{8}, \frac{\pi}{12}$, and $\frac{\pi}{20}$. Fig. 6(b), with ξ fixed at $\frac{\pi}{12}$, explores the effects of different plasma magnetization levels ($\sigma_0 = 5$, 10, 20,100) on the parameter space. The boundaries of the shaded regions in both subplots align with the relationship curves between a/M and ΛM^2 when the Kerr-AdS black hole represents an extremal black hole (as shown by the blue solid curve in Fig. 1). Observations reveal that a reduced orientation angle or increased plasma magnetization augments the shaded regions, broadening the feasible ranges of a/M and ΛM^2 for energy extraction. It is noteworthy that for fixed values of orientation angle ξ or plasma magnetization σ_0, the viable range of a/M for energy extraction initially expands and then contracts as ΛM^2 decreases from 0. This observation underscores that Kerr-AdS black holes empower plasma to extract energy even at significantly lower spin values (e.g., $a/M = 0.86$), a feat unattainable by Kerr black holes ($\Lambda M^2 = 0$).

This discovery introduces an important opportunity for plasma to extract energy from black holes characterized by lower spin parameters, showcasing the unique capabilities of Kerr-AdS black holes in this energy extraction context.

V. ENERGY EXTRACTION EFFICIENCY AND POWER

In the previous section, we calculated the hydrodynamic energy-at-infinity per enthalpy $\epsilon_{\pm}^{\infty}$ of the plasma,

encompassing the vicinity of a Kerr-AdS black hole. Subsequently, we derived the conditions necessary for energy extraction, followed by an exploration of the parameter space that satisfies these energy extraction conditions, demonstrating the practicality of extracting energy from Kerr-AdS black holes. To further consider the plasma's capacity for extracting energy from a Kerr-AdS black hole, our investigation will now delve into evaluating the efficiency and power associated with this energy extraction process.

Now, we examine the efficiency of extracting energy from the Kerr-AdS black hole through the mechanism of magnetic reconnection. The efficiency of this energy extraction process can be defined by the following equation [18]:

$$\eta = \frac{\epsilon_+^{\infty}}{\epsilon_+^{\infty} + \epsilon_-^{\infty}}. \tag{29}$$

From (29), we can conclude that energy will be extracted from the Kerr-AdS black hole only when $\eta > 1$.

Building on the insights from Ref. [18], we investigate the efficiency η of energy extraction as a function of the dominant reconnection radial position r/M for Kerr-AdS black holes, maintaining a constant plasma magnetization of $\sigma_0 = 100$ and reconnection angle $\xi = \frac{\pi}{12}$. In Fig. 7(a), with the cosmological constant fixed at $\Lambda M^2 = -0.01$, the efficiency η displays non-monotonic behavior across all tested spin values a/M. It exhibits an initial ascent followed by a descent as r/M increases, with peak values occurring in proximity to the circular corotating photon orbit. Notably, higher values of a/M correspond to larger peak efficiencies η, underlining the enhanced energy extraction potential with increasing black hole spin.

Examining Fig. 7(b) with $a/M = 0.99$, a similar behavior is observed where the efficiency η initially rises and then decreases as r/M varies across different cosmological constant values ΛM^2. The peak efficiency for η is consistently obtained when the dominant reconnection radial locations are closer to the circular corotating photon orbit. Furthermore, lower values of a/M correspond to higher peak efficiencies η. Remarkably, the Kerr black hole scenario ($\Lambda M^2 = 0$) achieves the smallest peak efficiency η. This comparison underscores the significantly enhanced energy extraction capability of plasma in Kerr-AdS black holes compared to Kerr black holes, particularly when the reconnection occurs in the vicinity of critical photon orbits. This enhanced energy extraction strength further accentuates as the cosmological constant ΛM^2 decreases.

Subsequently, in Fig. 8, we set the spin at $a/M = 0.99$, plasma magnetization at $\sigma_0 = 100$, and orientation angle at $\xi = \frac{\pi}{12}$ to examine the efficiency η as a function of the cosmological constant ΛM^2 across various dominant reconnection radial locations r/M. The efficiency demonstrates distinct behaviors with the specific radial position of dominant reconnection. At smaller radii, like $r/M = 1.25$, η exhibits a continuous decrease as ΛM^2. When the radial position slightly increases, for example, at $r/M = 1.35$, η initially rises and then falls with ΛM^2, as depicted in Fig. 8(b). In contrast, at larger radial positions such as $r/M = 1.75$, η consistently rises with ΛM^2. Nonetheless, across all scenarios, a lower cosmological constant correlates with higher efficiency η, indicating a more robust energy extraction capability. These results emphasize the significance of the dominant reconnection radial position in modulating the efficacy of energy extraction, with lower radial positions favoring heightened energy extraction. However, when r/M is extremely small, such as 1.15, the value of η precipitously drops below one as the cosmological constant increases.

Another crucial aspect in evaluating the potential for energy extraction from Kerr-AdS black holes via magnetic reconnection is the power of energy extraction. The power $P_{\rm extr}$ denotes the rate at which the plasma escapes

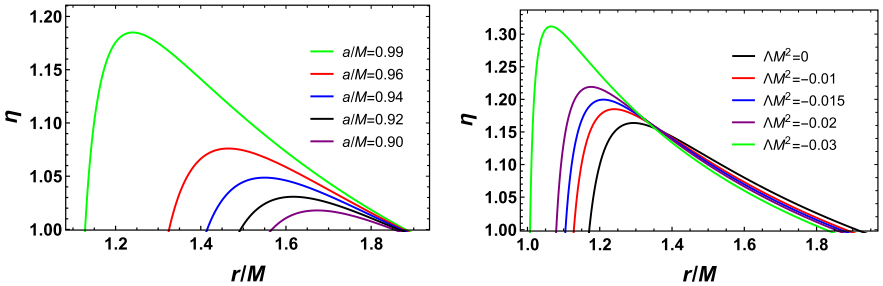

(a) $\Lambda M^2 = -0.01$ (b) $a/M = 0.99$

Fig. 7. (color online) (a) Behaviors of η as a function of the dominant reconnection radial location r/M by taking $\sigma_0 = 100$, $\xi = \frac{\pi}{12}$, and $\Lambda M^2 = -0.01$ with different values of spin a/M. Spin a/M = 0.99, 0.96, 0.94, 0.92, and 0.90 from top to bottom. (b) The behaviors of η as a function of the dominant reconnection radial location r/M by taking $\sigma_0 = 100$, $\xi = \frac{\pi}{12}$, and $a/M = 0.99$ with different values of the cosmological constant ΛM^2. Cosmological constant ΛM^2 = -0.03, -0.02, -0.015, -0.01, and 0 from top to bottom.

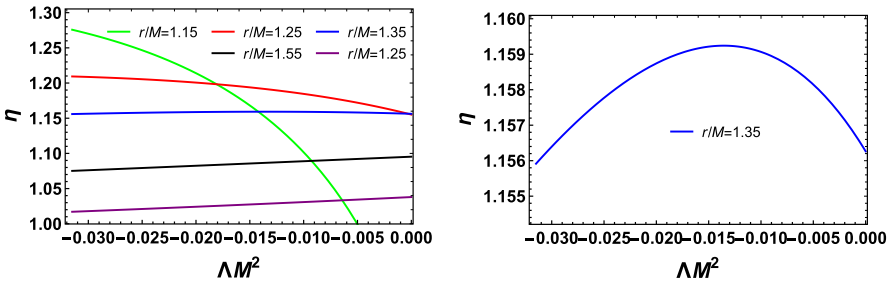

(a) $\sigma_0 = 100$, $\xi = \frac{\pi}{12}$, $a/M = 0.99$ (b) $\sigma_0 = 100$, $\xi = \frac{\pi}{12}$, $a/M = 0.99$

Fig. 8. (color online) Behavior of efficiency η as a function of the cosmological constant ΛM^2 by taking $\sigma_0 = 100$, $\xi = \frac{\pi}{12}$, and $a/M = 0.99$ with different dominant reconnection radial location r/M. (b) shows the behavior of η when r/M is set to 1.35 in (a).

the black hole to extract energy from it and can be defined as [18]

$$P_{\rm extr} = -\epsilon^{\infty}_{-}\omega_0 A_{\rm in} U_{\rm in}, \tag{30}$$

where $A_{\rm in}$ denotes the cross-sectional area of the inflowing plasma, which for rapidly spinning black holes is approximately $A_{\rm in} \sim (r^2_{\rm E} - r^2_{\rm LR})$. The plasma inflow four-velocity is represented by $U_{\rm in}$, typically $U_{\rm in} = O(10^{-1})$ for the collisionless regime and $U_{\rm in} = O(10^{-2})$ for the collisional regime, as discussed in [76], with $U_{\rm in}$ set at 0.1 for this analysis. Consequently, the power per unit enthalpy can be furhter expressed as

$$P_{\rm extr}/\omega_0 = -0.1\epsilon^{\infty}_{-}(r^2_{\rm E} - r^2_{\rm LR}). \tag{31}$$

We consider a black hole spin of $a/M = 0.99$ and illustrate the power $P_{\rm extr}/\omega_0$ as a function of the dominant reconnection radial location r/M in Fig. 9. Figs. 9(a) and 9(b) display the behavior of $P_{\rm extr}/\omega_0$ with increasing r/M for various orientation angles ξ under cosmological constant values of $\Lambda M^2 = 0$ and $\Lambda M^2 = -0.03$, respectively. Additionally, Figs. 9(c) and 9(d) showcase the behavior of $P_{\rm extr}/\omega_0$ with increasing r/M for different plasma magnetization σ_0 under cosmological constant values of $\Lambda M^2 = 0$ and $\Lambda M^2 = -0.03$, respectively. Note that $\Lambda M^2 = 0$ denotes the scenario of a Kerr black hole. From

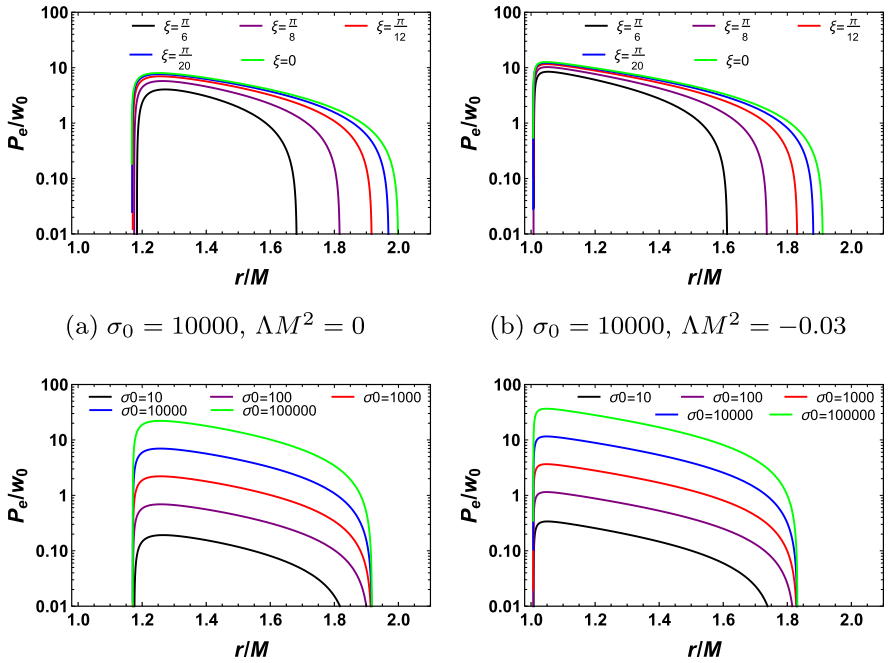

(a) $\sigma_0 = 10000$, $\Lambda M^2 = 0$ (b) $\sigma_0 = 10000$, $\Lambda M^2 = -0.03$

(c) $\xi = \frac{\pi}{12}$, $\Lambda M^2 = 0$ (d) $\xi = \frac{\pi}{12}$, $\Lambda M^2 = -0.03$

Fig. 9. (color online) Log-plot of the power $P_{\rm extr}/\omega_0$ as a function of the dominant reconnection radial location r/M with $a/M = 0.99$ and $\Lambda M^2 = -0.01$. (a), (b) Plasma magnetization $\sigma_0 = 10$ and orientation angles $\xi = \frac{\pi}{6}, \frac{\pi}{8}, \frac{\pi}{12}, \frac{\pi}{20}, 0$ from bottom to top. (c), (d) Orientation angle $\xi = \frac{\pi}{12}$ and plasma magnetization $\sigma_0 = 10$, 100, 1000, 10000, 100000 from bottom to top.

these subplots, it is evident that the power $P_{\rm extr}/\omega_0$ peaks at an r/M value in close proximity to the dominant reconnection radial location near the circular corotating photon orbit, following which it decreases with further increments in r/M. A smaller orientation angle ξ or a higher plasma magnetization σ_0 correlates with increased energy extraction power $P_{\rm extr}/\omega_0$. Comparative analysis between plots with $\Lambda M^2 = 0$ and $\Lambda M^2 = -0.03$ reveals that a reduction in the cosmological constant ΛM^2 reduces the radius of the co-rotating photon circular orbit, shifting the peak towards smaller r/M values while intensifying the peak of $P_{\rm extr}/\omega_0$. This observation strongly suggests that the presence of a negative cosmological constant enhances the plasma's capability to extract energy from the black hole.

To further illustrate the impact of the cosmological constant on the power dynamics, we present the power $P_{\rm extr}/\omega_0$ as a function of the cosmological constant ΛM^2 across different dominant reconnection radial locations r/M. This analysis is conducted with $a/M = 0.99$, $\sigma_0 = 10000$, and $\xi = \frac{\pi}{12}$, as depicted in Fig. 10. Fig. 10(b) provides a detailed breakdown of the power behavior in relation to ΛM^2 when r/M is set to 1.4, as shown in Fig. 10(a). When r/M is relatively small, e.g., $r/M = 1.2$, the power $P_{\rm extr}/\omega_0$ exhibits a consistent decrease with increasing ΛM^2. At $r/M = 1.4$, Fig. 10(b) illustrates that as ΛM^2 increases, $P_{\rm extr}/\omega_0$ initially decreases before transiting to an increase. Considering larger values of r/M, exemplified by $r/M = 1.8$, $P_{\rm extr}/\omega_0$ demonstrates a continuous increase alongside the increase in ΛM^2. In general, when the dominant reconnection radial location r/M is smaller, the power $P_{\rm extr}/\omega_0$ tends to be higher, with lower values of ΛM^2 corresponding to increased $P_{\rm extr}/\omega_0$. This observation underscores the intricate relationship between the dominant reconnection radial position, cosmological constant, and power dynamics of energy extraction from Kerr-AdS black holes.

Finally, for a comprehensive comparison of the energy extraction efficiency between plasma in Kerr-AdS and Kerr black holes via the magnetic reconnection mechanism, we introduce the energy extraction power ratio κ as [18]

$$\kappa = \frac{P^{\rm Kerr-AdS}_{\rm extr}}{P^{\rm Kerr}_{\rm extr}}. \tag{32}$$

For $P^{\rm Kerr}_{\rm extr}$, we only need to substitute $\Lambda M^2 = 0$ into (30).

In Fig. 11, we fix the spin at $a/M = 0.99$, $\sigma_0 = 10000$, and $\xi = \frac{\pi}{12}$ and then illustrate the power ratio κ as a function of the cosmological constant ΛM^2 across various dominant reconnection radial locations r/M. The behavior reveals that for smaller dominant reconnection radial locations, such as $r/M < 1.5$, κ surpasses one, with a smaller cosmological constant ΛM^2 resulting in a higher κ. This observation suggests that energy extraction from a Kerr-AdS black hole is more efficient than that from a Kerr black hole, with the presence of the cosmological constant ΛM^2 amplifying the efficacy of magnetic reconnection for energy extraction. However, when r/M is relatively large, as exemplified by the value 1.7, $\kappa < 1$. In such instances, the Kerr-AdS black hole does not offer a notable advantage in energy extraction compared to a Kerr black hole. In conclusion, the dominant reconnection radial location r/M significantly impacts the energy extraction from Kerr-AdS black holes through the magnetic reconnection mechanism. Notably, plasma demonstrates a substantial edge in energy extraction at smaller r/M positions within Kerr-AdS black holes in contrast to Kerr black holes.

Meanwhile, to further highlight the unique role of the cosmological constant on energy extraction by magnetic reconnection, we calculate the following energy extraction power ratio to compare the energy extraction power of Kerr-dS black holes with a positive cosmological constant and Kerr-AdS black holes with a negative cosmological constant:

$$\kappa = \frac{P^{\rm Kerr-dS}_{\rm extr}}{P^{\rm Kerr-AdS}_{\rm extr}}, \tag{33}$$

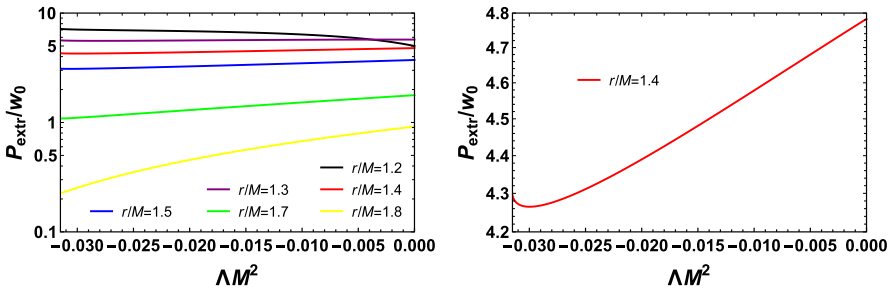

(a) $\sigma_0 = 10000$, $\xi = \frac{\pi}{12}$, $a/M = 0.99$ (b) $\sigma_0 = 10000$, $\xi = \frac{\pi}{12}$, $a/M = 0.99$

Fig. 10. (color online) (a) Log-plot of power $P_{\rm extr}/\omega_0$ as a function of cosmological constant ΛM^2 with different dominant reconnection radial location by taking $a/M = 0.99$, $\sigma_0 = 10000$, and $\xi = \frac{\pi}{12}$. (b) shows the behavior of $P_{\rm extr}/\omega_0$ when $r/M = 1.4$ in (a).

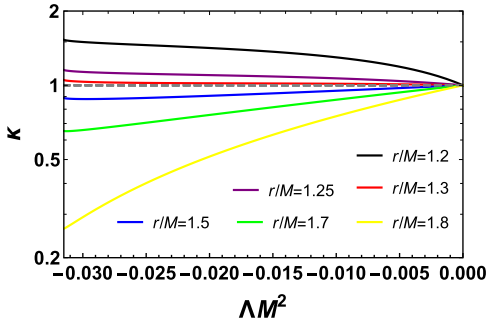

Fig. 11. (color online) Behavior of power ratio κ as a function of cosmological constant ΛM^2 with different dominant reconnection radial location by taking $a/M=0.99$, $\sigma_0=10000$, and $\xi=\frac{\pi}{12}$.

where $P^{\rm Kerr-dS}_{\rm extr}$ has been discussed in detail in Ref. [33].

By fixing $a/M=0.99$, $\sigma_0=10000$, and $\xi=\frac{\pi}{12}$ in Fig. 12, we observe the power ratio κ as a function of the dominant reconnection radial location r/M. Curves of different colors represent Kerr-dS and Kerr-AdS black holes with different values of the cosmological constant. For example, $|\Lambda M^2|=0.03$ denotes $\Lambda M^2=0.03$ for Kerr-dS black holes and $\Lambda M^2=-0.03$ for Kerr-AdS black holes. From Fig. 12, we can see that as the dominant reconnection radial location increases, κ shows an upward trend. This indicates that during the increase of the dominant reconnection radial location, the advantage of energy extraction in Kerr-dS black holes gradually improves compared to that in Kerr-AdS black holes. However, when the dominant reconnection radial location is relatively small, such as $r/M<1.35$, κ is consistently less than 1. This suggests that in Kerr-AdS black holes, the energy extraction power is greater, making energy extraction more favorable than in Kerr-dS black holes. Moreover, at smaller r/M, when the cosmological constant ΛM^2 for Kerr-AdS is smaller, for example $\Lambda M^2=-0.03$, κ becomes even smaller. In this case, the

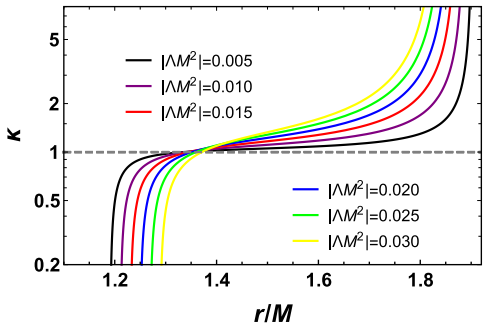

Fig. 12. (color online) Behavior of power ratio κ as a function of the dominant reconnection radial location r/M with values of different cosmological constant by taking $a/M=0.99$, $\sigma_0=10000$, and $\xi=\frac{\pi}{12}$.

advantage of energy extraction in Kerr-AdS black holes is further enhanced compared to that in Kerr-dS black holes. In contrast, at larger dominant radial positions, such as $r/M>1.7$, κ is significantly greater than 1. Here, the advantage of energy extraction in Kerr-dS black holes is markedly stronger than in Kerr-AdS black holes, and for Kerr-dS black holes, a larger cosmological constant ΛM^2 corresponds to a larger κ.

Above, we calculated the ratio of energy extraction power, comparing the power of energy extraction in Kerr-AdS black holes with that in Kerr and Kerr-dS black holes. We conclude that when the dominant reconnection radial location of magnetic reconnection is relatively small and the negative cosmological constant ΛM^2 is smaller, energy extraction in Kerr-AdS black holes shows a significant advantage compared to that in Kerr and Kerr-dS black holes.

VI. CONCLUSIONS AND DISCUSSIONS

As predicted by general relativity, spinning black holes possess considerable energy. Since Penrose introduced the Penrose process for extracting rotational energy from spinning black holes, various energy extraction mechanisms have been explored to elucidate high-energy astrophysical phenomena. Comisso and Asenjo conducted an in-depth study on extracting energy from Kerr black holes using magnetic reconnection. This study extended the investigation to Kerr-AdS black holes with negative cosmological constants, examining the viability of energy extraction through magnetic reconnection in this context.

Given that energy extraction occurs within a black hole's ergosphere, we initially analyzed the spacetime structure and characteristic radii of Kerr-AdS black holes. By studying the event horizon, we delineated the parameter space $\Lambda M^2-a/M$ allowing for Kerr-AdS black hole existence. Notably, as the spin decreases, the minimum negative cosmological constant value also decreases, approaching negative infinity with a Kerr-AdS black hole spin nearing 0. Research on the outer ergosphere boundary and circular corotating photon orbit revealed how these characteristic radii vary with ΛM^2 or a/M. The radii values increase with cosmological constant under fixed spin conditions and decrease with spin under fixed cosmological constant.

Subsequently, we calculated the hydrodynamic energy-at-infinity per plasma enthalpy $\epsilon^{\infty}_{\pm}$ around Kerr-AdS black holes, deriving conditions for energy extraction. Plotting ϵ^{∞}_{+} and ϵ^{∞}_{-} as functions of spin a/M, cosmological constant ΛM^2, magnetization σ_0, orientation angle ξ, and dominant reconnection radial location r/M emphasizes the dependence of Kerr-AdS black hole energy extraction via magnetic reconnection on ϵ^{∞}_{-}. Notably, greater spin a/M, higher plasma magnetization σ_0, and smal-

ler azimuthal angles ξ enable more efficient energy extraction, akin to observations in Kerr black holes. The impact of cosmological constant ΛM^2 on energy extraction is influenced by dominant reconnection radial location r/M. Notably, at smaller r/M, energy extraction from Kerr-AdS black holes surpasses that from Kerr black holes, with extractable energy increasing as ΛM^2 decreases.

Then, we delineated parameter space regions $\Lambda M^2 - r/M$ and $a/M - \Lambda M^2$ satisfying energy extraction conditions. Higher plasma magnetization σ_0 and lower orientation angle ξ widen the permissible ranges of spin a/M, cosmological constant ΛM^2, and dominant reconnection radial location r/M for energy extraction from Kerr-AdS black holes. Negative cosmological constants expand the feasible a/M and r/M ranges, enabling energy extraction from low-spin black holes.

To further evaluate plasma's energy extraction capability from Kerr-AdS black holes through magnetic reconnection, we calculated the efficiency η and power $P_{\rm extr}/\omega_0$. Enhanced plasma magnetization σ_0 and reduced orientation angle ξ lead to higher efficiency and power. Notably, energy extraction power and efficiency peak at smaller r/M, with efficiencies not consistently increasing or decreasing with ΛM^2 changes. By comparing the energy extraction capabilities of Kerr-AdS black holes with that of Kerr and Kerr-dS black holes via magnetic reconnection using power ratio κ, we found that at smaller dominant reconnection radial locations, compared with Kerr and Kerr-dS black holes, Kerr-AdS black holes exhibit a more superior energy extraction advantage. Moreover, as the negative cosmological constant of the Kerr-AdS black hole decreases, the energy extraction capability further enhances.

In summary, this study demonstrated the feasibility of extracting energy from Kerr-AdS black holes and underscores the significant impact of negative cosmological constants on black hole energy extraction via magnetic reconnection. The presence of negative cosmological constants expands the permissible dominant reconnection radial locations for meeting energy extraction conditions, facilitating energy extraction from low-spin black holes. The influence of negative cosmological constants on energy extraction is modulated by dominant reconnection radial location, with more energy extractable at smaller r/M, particularly as ΛM^2 decreases. Energy extraction from Kerr-AdS black holes proves more advantageous than that from Kerr and kerr-dS black holes via magnetic reconnection.

Future work may explore energy extraction from Kerr-AdS black holes through the collisional Penrose process, BSW acceleration mechanism, and Blandford-Znajek mechanism by comparing these with magnetic reconnection-based energy extraction. Additionally, investigations into energy extraction from other rotating black hole types, such as higher-dimensional rotating black holes [77], could offer further insights into energy extraction mechanisms.

References

[1] B. P. Abbott *et al.* (LIGO Scientific and Virgo Collaborations), Phys. Rev. Lett. **116**, 061102 (2016), arXiv: 1602.03837[gr-qc]

[2] B. P. Abbott *et al.* (LIGO Scientific and Virgo Collaborations), Phys. Rev. Lett. **119**, 161101 (2017), arXiv: 1710.05832[gr-qc]

[3] B. P. Abbott *et al.* (LIGO Scientific Collaboration), Rept. Prog. Phys. **72**, 076901 (2009), arXiv: 0711.3041[gr-qc]

[4] K. Akiyama *et al.* (Event Horizon Telescope Collaboration), Astrophys. J. Lett. **875**, L1 (2019), arXiv: 1906.11238

[5] K. Akiyama *et al.* (Event Horizon Telescope Collaboration), Astrophys. J. Lett. **930**, L17 (2022), arXiv: 2311.09484

[6] B. M. Peterson, *An Introduction to Active Galactic Nuclei*, (Cambridge: Cambridge University Press, 1997).

[7] J. C. McKinney and C. F. Gammie, Astrophys. J. **611**, 977 (2004), arXiv: astro-ph/0404512

[8] M. C. Bentz and S. Katz, PASP **127**, 67 (2015), arXiv: 1411.2596[astro-ph.GA]

[9] F. Combes, *Active Galactic Nuclei: Fueling and feedback*, (IOP Publishing, 2021).

[10] R. Narayan, A. Sadowski, and R. Soria, Mon. Not. Roy. Astron. Soc. **469**, 2997 (2017), arXiv: 1702.01158[astro-ph.HE]

[11] M. Bachetti, Astron. Nachr. **337**, 349 (2017), arXiv: 1510.05565

[12] M. D. Caballero-Garcia and A. C. Fabian, Mon. Not. Roy. Astron. Soc. **402**, 2559 (2010), arXiv: 0910.2418

[13] R. Penrose, Riv. Nuovo Cim. **1**, 252 (1969)

[14] T. Piran, J. Shaham, and J. Katz, Astrophys. J. Lett. **196**, L107 (1975)

[15] M. Banados, J. Silk, and S. M. West, Phys. Rev. Lett. **103**, 111102 (2009), arXiv: 0909.0169[hep-ph]

[16] R. D. Blandford and R. L. Znajek, Mon. Not. Roy. Astron. Soc. **179**, 433 (1977)

[17] S. Koide and K. Arai, Astrophys. J. **682**, 1124 (2008), arXiv: 0805.0044[astro-ph]

[18] L. Comisso and F. A. Asenjo, Phys. Rev. D **103**, 023014 (2021), arXiv: 2012.00879

[19] K. Akiyama *et al.* (Event Horizon Telescope Collaboration), Astrophys. J. Lett. **910**, L12 (2021), arXiv: 2105.01169

[20] K. Akiyama *et al.* (Event Horizon Telescope Collaboration), Astrophys. J. Lett. **910**, L13 (2021), arXiv: 2105.01173

[21] S. S. Komissarov, Mon. Not. Roy. Astron. Soc. **359**, 801 (2005), arXiv: astro-ph/0501599

[22] W. E. East and H. Yang, Phys. Rev. D **98**, 023008 (2018), arXiv: 1805.05952

[23] K. Parfrey, A. Philippov, and B. Cerutti, Phys. Rev. Lett. **122**, 035101 (2019), arXiv: 1810.03613

[24] B. Ripperda, F. Bacchini, and A. Philippov, Astrophys. J. **900**, 100 (2020), arXiv: 2003.04330

[25] L. Comisso, M. Lingam, Y. M. Huang *et al.*, Phys. Plasmas **23**, 100702 (2016), arXiv: 1608.04692

[26] D. A. Uzdensky and N. F. Loureiro, Phys. Rev. Lett. **116**, 105003 (2016), arXiv: 1411.4295
[27] L. Comisso, M. Lingam, Y. M. Huang *et al*., Astrophys. J. **850**, 142 (2017), arXiv: 1707.01862
[28] D. Biskamp, *Magnetic Reconnection in Plasmas*, (Cambridge: Cambridge University Press, 2005).
[29] N. F. Loureiro, A. A. Schekochihin, and S. C. Cowley, Phys. Plasmas **14**, 100703 (2007), arXiv: astro-ph/0703631
[30] A. Bhattacharjee, Y. M. Huang, H. Yang *et al*., Phys. Plasmas **16**, 112102 (2009), arXiv: 0906.5599
[31] W. Daughton, V. Roytershteyn, B. J. Albright *et al*., Phys. Rev. Lett. **103**, 065004 (2009)
[32] S. W. Wei, H. M. Wang, Y. P. Zhang *et al*., JCAP **04**, 050 (2008), arXiv: 2201.12729[gr-qc]
[33] C. H. Wang, C. Q. Pang, and S. W. Wei, Phys. Rev. D **106**, 124050 (2022), arXiv: 2209.08837[gr-qc]
[34] A. Carleo, G. Lambiase, and L. Mastrototaro, Eur. Phys. J. C **82**, 776 (2022), arXiv: 2206.12988[gr-qc]
[35] M. Khodadi, D. F. Mota, and A. Sheykhi, JCAP **10**, 034 (2023), arXiv: 2307.00478
[36] Z. Li and F. Yuan, Phys. Rev. D **108**, 024039 (2023), arXiv: 2304.12553[gr-qc]
[37] S. J. Zhang, Phys. Rev. D **109**, 084066 (2024), arXiv: 2402.15050[gr-qc]
[38] W. Liu, Astrophys. J. **925**, 149 (2022), arXiv: 2204.07338
[39] Z. Li, X. K. Guo, and F. Yuan, Phys. Rev. D **108**, 044067 (2023), arXiv: 2304.08831[gr-qc]
[40] X. Ye, C. H. Wang, and S. W. Wei, JCAP **12**, 030 (2023), arXiv: 2306.12097[gr-qc]
[41] S. Shaymatov, M. Alloqulov, B. Ahmedov *et al*., Phys. Rev. D **110**, 044005 (2024), arXiv: 2307.03012[gr-qc]
[42] S. J. Zhang, JCAP **07**, 042 (2024), arXiv: 2405.16941[gr-qc]
[43] S. Rodriguez, A. Sidler, L. Rodriguez *et al*., Phys. Dark Univ. **48**, 101961 (2025), arXiv: 2407.15347[gr-qc]
[44] S. Shaymatov, Phys. Rev. D **110**, 044042 (2024), arXiv: 2402.02471[gr-qc]
[45] F. Long, S. Chen, S. Wang *et al*., Eur. Phys. J. C **85**, 26 (2025), arXiv: 2409.11942[gr-qc]
[46] B. Chen, Y. Hou, J. Li *et al*., Phys. Rev. D **110**, 063003 (2024), arXiv: 2405.11488[gr-qc]
[47] Y. Shen, H.-Y. YuChih, and B. Chen, Phys. Rev. D **110**, 123010 (2024), arXiv: 2409.07345[gr-qc]
[48] Y. Shen and H.-Y. YuChih, Phys. Rev. D **111**, 023003 (2025), arXiv: 2412.03010
[49] X. X. Zeng and K. Wang,Phys. Rev. D **112**, 064080 (2025), arXiv: 2507.10520 [gr-qc]
[50] Z. Cheng, S. Chen, and J. Jing,Eur. Phys. J. C **85**, 1130 (2025), arXiv: 2507.11859 [gr-qc]
[51] X. X. Zeng and K. Wang,Phys. Rev. D **112**, 064032 (2025), arXiv: 2507.21777 [gr-qc]
[52] K. Wang and X. X. Zeng, JCAP **11**, 026 (2025), arXiv: 2508.11934 [gr-qc]
[53] S. W. Hawking and G. F. R. Ellis, *The Large Scale Structure of Space-Time*, (Cambridge: Cambridge University Press, 1973).
[54] J. M. Maldacena, Adv. Theor. Math. Phys. **2**, 231 (1998), arXiv: hep-th/9711200[hep-th]
[55] E. Witten, Adv. Theor. Math. Phys. **2**, 253 (1998), arXiv: hep-th/9802150
[56] L. Susskind and E. Witten, (1998), arXiv: hep-th/9805114
[57] S. W. Hawking, C. J. Hunter, and M. Taylor, Phys. Rev. D **59**, 064005 (1999), arXiv: hep-th/9811056
[58] S. S. Gubser, I. R. Klebanov, and A. M. Polyakov, Phys. Lett. B **428**, 105 (1998), arXiv: hep-th/9802109[hep-th]
[59] S. W. Hawking and D. N. Page, Commun. Math. Phys. **87**, 577 (1983)
[60] E. Witten, Adv. Theor. Math. Phys. **2**, 505 (1998), arXiv: hep-th/9803131
[61] D. Kastor, S. Ray, and J. Traschen, Class. Quant. Grav. **26**, 195011 (2009), arXiv: 0904.2765[hep-th]
[62] S. Gunasekaran, D. Kubiznak, and R. Mann, JHEP **11**, 110 (2012), arXiv: 1208.6251
[63] S. W. Wei and Y. X. Liu, Phys. Rev. Lett. **115**, 111302 (2015), arXiv: 1502.00386[gr-qc]
[64] S. W. Wei, Y. X. Liu, and R. B. Mann, Phys. Rev. Lett. **123**, 071103 (2019), arXiv: 1906.10840[gr-qc]
[65] S. W. Wei, Y. X. Liu, and R. B. Mann, Phys. Rev. D **100**, 124033 (2019), arXiv: 1909.03887[gr-qc]
[66] B. Carter, Commun. Math. Phys. **10**, 280 (1968)
[67] E. Hackmann, C. Lämmerzahl, V. Kagramanova *et al*., Phys. Rev. D **81**, 044020 (2010), arXiv: 1009.6117 [gr-qc]
[68] A. Grenzebach, V. Perlick, and C. Lammerzahl, Phys. Rev. D **89**, 124004 (2014), arXiv: 1403.5234 [gr-qc]
[69] X. C. Cai and Y. G. Miao, (2021), arXiv: 2107.08352 [gr-qc]
[70] J. M. Bardeen, W. H. Press, and S. A. Teukolsky, Astrophys. J. **178**, 347 (1972)
[71] J. M. Bardeen, Astrophys. J. **162**, 71 (1970)
[72] K. S. Thorne, R. H. Price, and D. A. Macdonald, *Black holes: The membrane paradigm*, (Yale University Press, 1986).
[73] S. Koide, K. Shibata, and T. Kudoh, Astrophys. J. **522**, 727 (1999)
[74] R. Giacconi and R. Ruffini, *Physics and astrophysics of neutron stars and black holes*, (Amsterdam: North-Holland Publishing Company, 1978).
[75] T. Damour, R. S. Hanni, R. Ruffini *et al*., Phys. Rev. D **17**, 1518 (1978)
[76] L. Comisso and A. Bhattacharjee, J. Plasma Phys. **82**, 595820601 (2016), arXiv: 1609.02998
[77] R. C. Myers and M. J. Perry, Ann. Phys. **172**, 304 (1986)